International Journal of Thermophysics, Vol. 20, No. 2, 1999

The Nearly Classical Behavior of a Pure Fluid on the Critical Isochore Very Near the Critical Point Under the Influence of Gravity

N. Kurzeja,[1] Th. Tielkes,[2] and W. Wagner[1, 3]

Received May 1, 1998

Comprehensive measurements of the isothermal compressibility along the critical isochore in the critical region of pure sulfur hexafluoride (SF_6) and pure carbon dioxide (CO_2) were carried out. All measurements were performed with a multicell apparatus, especially designed for $p\rho T$ measurements in the critical region. The height of the measuring cells was either 30 or 11 mm. Independent of the cell height, we found for both fluids nearly "classical" values for the critical exponent γ in the limiting approach to the critical point. However, at a certain distance from the critical point $\{(T-T_c) \approx 90$ mK or $\tau \approx 2.82 \times 10^{-4}$ for SF_6 and $(T-T_c) \approx 55$ mK or $\tau \approx 1.81 \times 10^{-4}$ for $CO_2\}$, we observed a transition to values of the critical exponents which nearly meet the predictions of the renormalization-group theory. Since in the fitting range ($T-T_c \geqslant 1$ mK) the correlation length ($\xi \leqslant 0.5\,\mu$m) is very much smaller than the geometrical dimensions of the measuring cells, we conclude that the reason for the different behavior is an explicit gravity effect governing the inner critical region. The two different loci of the transition points for sulfur hexafluoride and carbon dioxide can be attributed to the different gravity impact on the fluid corresponding to the different critical densities of the two substances.

KEY WORDS: carbon dioxide; critical exponent; critical point; differential pressure; gravity; isothermal compressibility; multicell apparatus; sulfur hexafluoride.

1. INTRODUCTION

In order to measure the thermal behavior in the critical region of pure fluids considerably more accurately than had been previously possible,

[1] Lehrstuhl für Thermodynamik, Ruhr-Universität Bochum, D-44780 Bochum, Germany.
[2] Forschungs- und Technologiezentrum, Deutsche Bahn AG, D-80939 München, Germany.
[3] To whom correspondence should be addressed.

0195-928X/99/0300-0531$16.00/0

a new special $p\rho T$ multicell apparatus was developed [1, 2]. In 1990, we finished our first $p\rho T$ measurements in the critical region of sulfur hexafluoride (SF_6), which were the first comprehensive direct $p\rho T$ measurements in the really near-critical region. The results of these measurements were reported at the 11th Symposium on Thermophysical Properties in 1991 [3]. In the limiting approach to the critical point we found nearly classical values for the critical exponents β, γ, and δ. However, at a certain distance from the critical point we observed a transition to nonclassical behavior as predicted by the renormalization-group theory. Based on the corrections for density stratification, this transition point could be identified as the limit of significant gravity influence on the thermal behavior of SF_6. For a clarification of these results we have since then focused our efforts on a systematic investigation of this gravity influence.

In the first step we used new "horizontal" measuring cells with a height of only 11 mm in addition to the 30-mm-high cells. With these new cells we repeated our previous [3] measurements of the isothermal compressibility on the critical isochore of SF_6 and found nearly identical results for γ [4].

In the second step we varied the fluid itself and performed comprehensive $p\rho T$ measurements in the critical region of carbon dioxide (CO_2) and again studied the isothermal compressibility along the critical isochore. For cell heights of both 30 and 11 mm, the new results for CO_2 are in remarkable agreement with the results obtained for SF_6. A detailed description of these measurements is given in separate papers [5–8].

In this paper we concentrate only on the measurements of the isothermal compressibility which we performed along the critical isochore, both on SF_6 and on CO_2.

2. EXPERIMENTAL

The measuring principle and the design of the multicell apparatus with its four-stage high-precision thermostat were described in a previous paper [3]. The reason for creating this special $p\rho T$ multicell apparatus was to attain an extremely high internal consistency of the single $p\rho T$ measuring points with regard to temperature, pressure, and density. For this reason, not only one single measuring cell, but also a whole block of measuring cells, was built into a high-precision thermostat. The isothermal pressure differences between the cells filled with a fluid of different density are directly measured with high-precision differential pressure indicators (DPI). For measurements of the isothermal compressibility the two arrangements of measuring cells shown in Fig. 1 were used.

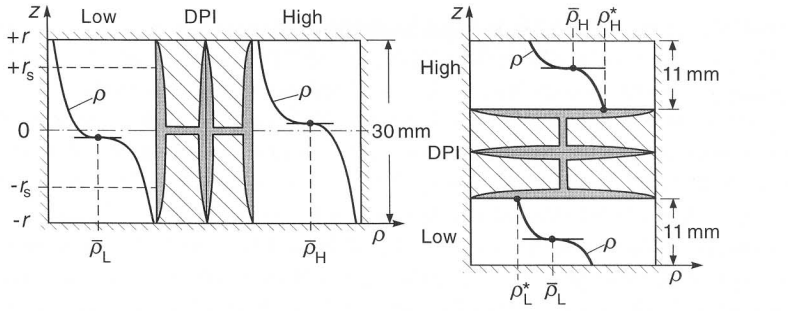

Fig. 1. Schematic design of a set of horizontal and a set of vertical measuring cells with a directly flanged differential pressure indicator (DPI). The density profiles shown inside the cells were calculated for a difference of $\pm 5\ \mathrm{kg \cdot m^{-3}}$ to the critical density just on the critical isotherm. Additional information is given in Appendix A.

In order to vary the height of the measuring cells the differential pressure indicator is either horizontally or vertically aligned. In the latter case the cell height is given by the diameter of the membranes of the DPI. The DPIs are directly flanged to the cells via metal-lip seals. Not shown in Fig. 1 are the all-metal valves also directly integrated with the measuring cell. We have designed two different blocks of measuring cells composed of either vertical or vertical and horizontal cells. Both blocks fit within our high-precision thermostat and meet the extreme requirements for the temperature gradients given by the isothermal principle of measuring isothermal compressibilities. The temperature stability with regard to time is better than $\pm 10\,\mu$K (over hours) and $\pm 25\,\mu$K (over days). As verified by several measurements (exchanging the locations of 25-Ω platinum thermometers), the temperature gradient over the entire block of measuring cells is smaller than $\pm 35\,\mu$K; therefore, over a single cell the gradient can be estimated to be smaller than $\pm 10\,\mu$K. For measuring and controlling the absolute temperature we use 25-Ω platinum resistance thermometers and AC resistance bridges. In this way we achieved a consistency of the temperature measurements of better than $\pm 25\,\mu$K and an uncertainty in the absolute temperature of less than ± 1 mK. All temperatures are reported on ITS-90.

The process of filling the measuring cells with the fluid of desired density is based on $p\rho T$ data measured by Gilgen et al. [9] for SF_6 and by Nowak et al. [10] for CO_2. When taking into account the uncertainty of the densities from Refs. 9 and 10, and the change in cell volume due to time, temperature, pressure, and displacement of the membranes of the differential pressure indicators, the Gaussian error propagation leads to an

uncertainty of the actual density within the measuring cells of $\Delta\rho/\rho \leqslant \pm 5 \times 10^{-4}$; the corresponding value for the consistency of the actual densities along two isochores is estimated to be $\Delta\rho/\rho \leqslant \pm 1 \times 10^{-4}$.

The total uncertainty of the determined differential pressure is based on three influences: the uncertainty of the differential pressure indicators, the uncertainty of the calibration, and the uncertainty of the corrections for the averaging error, the so-called implicit gravity influence. The uncertainty of the DPIs was minimized by a special mathematical model to take into account the influences of temperature, absolute pressure, and time. A newly developed differential pressure standard [$\Delta(\Delta p) \leqslant \pm 2$ Pa, $p_{\max} \leqslant 10$ MPa; see Ref. 5] was used for careful calibration of the DPIs. The averaging error was corrected by computing the density stratification with suitable equations of state (see Appendix A or Refs. 3 and 5). In this way, for the differential pressure measured between two cells we obtained a consistency of better than ± 0.2 Pa (± 0.5 Pa for the vertical cells with CO_2); this value includes the contributions to the differential pressure by the residual changes in density after the necessary volume corrections. The absolute uncertainty of the differential pressure over the whole range of 0 to 7500 Pa was $\Delta(\Delta p) \leqslant \pm 6$ Pa.

With these consistencies and uncertainties in the measured values of temperature, differential pressure, and density, it was possible to determine very consistent and precise values of the isothermal compressibility along the critical isochore. For this purpose, a set of either two vertical or two horizontal measuring cells (see Fig. 1) was filled "symmetrically around the critical density," which means that the fluid density in one of the two cells was slightly above the critical density, and in the other cell, the density was slightly below the critical density. The isothermal compressibility K_T is then obtained by the relation,

$$K_T = \frac{1}{\rho}\left(\frac{\partial \rho}{\partial p}\right)_T \approx \frac{1}{\bar{\rho}}\left(\frac{\Delta \rho}{\Delta p}\right)_T \tag{1}$$

where $\bar{\rho}$ is the averaged density of the two cells and $\Delta\rho$ and Δp are the differences in density and pressure, respectively, between the two cells; Δp is directly measured with the DPI but still has to be corrected for the implicit gravity effect (averaging error; see Appendix A).

The sulfur hexafluoride used for the measurements was supplied by Air Products (Germany). It was further purified by ourselves with a three-stage procedure. The procedure was started with the fluid phase of the delivered sample. The components H_2O and O_2 were removed by means of an appropriate molecular sieve and activated chromtrioxide (Oxisorb; Messer Griesheim, Germany), respectively. The low-boiling portion of the

impurities such as He, N_2, and CF_4 was removed by twice pumping off the gaseous phase above the frozen sample after a very slow desublimation (mass flow $\leqslant 0.0015\ g \cdot s^{-1}$) of the whole sample at about 1 K below the triple-point temperature of SF_6. Analyses performed by Linde (Germany) before and after the measurements did not yield any detectable impurities [$x(N_2) \leqslant 1 \times 10^{-6}$, $x(O_2) \leqslant 1 \times 10^{-6}$, $x(CF_4) \leqslant 1 \times 10^{-6}$, $x(He) \leqslant 0.5 \times 10^{-6}$, $x(H_2O) \leqslant 1 \times 10^{-6}$, and x(hydrocarbons) $\leqslant 1 \times 10^{-6}$, where x denotes mole fraction]. We expect the achieved purity to be $x(SF_6) \geqslant 0.999994$. The carbon dioxide was supplied by Messer Griesheim (Germany), with a certified purity of $x(CO_2) \geqslant 0.999999$. Again, the fluid was analyzed before and after the measurements by Messer Griesheim and no detectable impurities were found [$x(N_2) \leqslant 0.2 \times 10^{-6}$, $x(O_2) \leqslant 0.2 \times 10^{-6}$, $x(CO) \leqslant 0.01 \times 10^{-6}$, $x(He) \leqslant 0.5 \times 10^{-6}$, $x(H_2O) \leqslant 0.3 \times 10^{-6}$, x(hydrocarbons) $\leqslant 0.01 \times 10^{-6}$]. We emphasize the importance of the procedure to analyze the fluid used for the measurements before and after the measurements; due to the strong influence of impurities on the critical temperature T_c, only in this way can reliable values for the critical temperature be obtained.

3. RESULTS

The critical exponent γ is defined by the simple power law

$$K_T = \Gamma \left(\frac{T - T_c}{T_c} \right)^{-\gamma} \tag{2}$$

and can be determined by nonlinear fitting of the parameters Γ, T_c, and γ to the experimental values of the isothermal compressibility K_T along the critical isochore. However, to show the universal behavior of the isothermal compressibility we consider it advisable to use this equation in its dimensionless form,

$$p_c K_T = p_c \Gamma \left(\frac{T - T_c}{T_c} \right)^{-\gamma} \tag{3}$$

where p_c is the critical pressure. A quite usual visualization of the limiting behavior of the isothermal compressibility is given when plotting these data in a $p_c K_T$ vs $(T - T_c)/T_c$ diagram with a double-logarithmic scale. Figures 2 and 3 show such diagrams for our most reliable results of SF_6 (513 data points) and of CO_2 (231 data points).

When plotting the results of corresponding optical experiments [11–16] in such diagrams, all data would show the same slope, which means that they could be represented by *one* straight line. However, Figs. 2

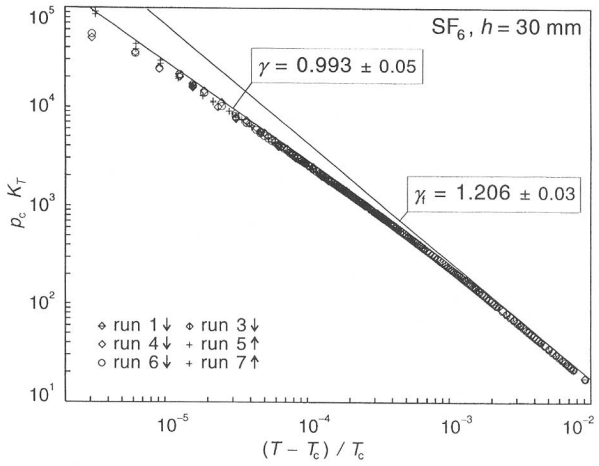

Fig. 2. Dimensionless isothermal compressibility $p_c K_T$ plotted vs the dimensionless temperature difference $(T - T_c)/T_c$ for the most reliable K_T data of SF_6. Runs recorded with decreasing temperature are characterized by the symbol ↓ just behind the run number; runs recorded with increasing temperature are characterized by the symbol ↑. Additional information on individual runs is given in Tables I and II.

and 3 show that our K_T data cannot be represented by one straight line since there are *two* ranges of different slopes, namely, the far-critical data not influenced by gravity with $\gamma = 1.206$ (SF_6) and $\gamma = 1.192$ (CO_2) and the gravity-influenced near-critical data with $\gamma = 0.993$ (SF_6) and $\gamma = 0.982$ (CO_2). For both fluids the experimental K_T data begin to deviate from the far-critical slope as soon as the calculated corrections for the averaging error exceed the statistical error of these calculations of ± 0.02 Pa. In the case of SF_6 this happens, however, at a greater distance to the critical point than in the case of CO_2. In order to give values of γ for the far-critical region in Figs. 2 and 3, which are truly not influenced by gravity, we restricted the lower limit of the far-critical fitting range to about $\tau > 2 \times 10^{-3}$ in the case of SF_6 and to about $\tau > 1 \times 10^{-3}$ in the case of CO_2. However, with only minor changes ($\Delta\gamma \approx 0.01$) in the values of the fitted exponent γ of Eq. (3) and some greater changes in the fitted critical temperature T_c, it is possible to extend the lower limit of the fitting range of the far-critical data to temperatures closer to T_c up to a so-called transition point, see below. The inclusion of data below this point into the fit leads to significantly smaller values of the fitted exponent γ. Therefore, this transition point characterizes the crossover from the far-critical to the near-critical fitting range, which is significantly influenced by gravity. Significantly

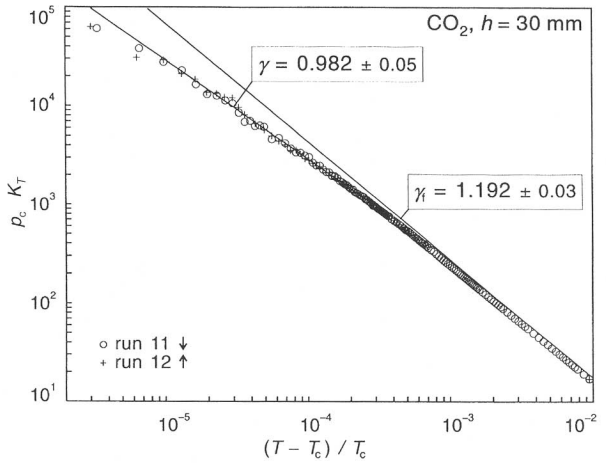

Fig. 3. Dimensionless isothermal compressibility $p_c K_T$ plotted vs the dimensionless temperature difference $(T - T_c)/T_c$ for the most reliable K_T data of CO_2. Runs recorded with decreasing temperature are characterized by the symbol ↓ just behind the run number; runs recorded with increasing temperature are characterized by the symbol ↑. Additional information on individual runs is given in Tables III and IV.

means that the corrections for the averaging error contribute more than about 5% to the differential pressures. For the two fluids considered, this crossover takes place at a different distance to the respective critical point; details are given below.

First we discuss, by means of Fig. 2, whether the differences between the near- and the far-critical slopes are truly outside the uncertainty of our experimental data. For this purpose, in Fig. 2 the K_T data for SF_6 of three statistically independent fillings of the vertical measuring cells with four average densities $\bar{\rho}$ are shown: run 1↓ with $\bar{\rho} = 744.3\ \mathrm{kg \cdot m^{-3}}$, run 3↓ with $\bar{\rho} = 745.5\ \mathrm{kg \cdot m^{-3}}$, run 4↓ and run 5↑ with $\bar{\rho} \approx 739.9\ \mathrm{kg \cdot m^{-3}}$, and run 6↓ and run 7↑ with $\bar{\rho} \approx 744.9\ \mathrm{kg \cdot m^{-3}}$ (see Table I). For each filling there are two separate determinations of the filled-in densities and the volume changes in the course of the measurements, as well as two independent calibrations of the DPIs and platinum resistance thermometers. Moreover, the measurements for each average density were carried out in different ranges of differential pressure. The agreement between the measurements with these four different fillings is astonishingly good. Furthermore, run 4↓ and run 6↓ are equivalent to run 5↑ and run 7↑, respectively, but they were recorded 4 months later with the starting point of the measurements in the two-phase region instead of as previously on the reference isotherm

Table I. Fitting of Eq. (3) to the Experimental K_T Data for Sulfur Hexafluoride (Inner Region)

Run	Cells	$\bar{\rho}$ (kg · m^{-3})	$\Delta\rho$ (kg · m^{-3})	Temperature range (mK)	Data points	T_c (K)	$p_c\Gamma$	γ
1↓	Vert.	744.311	14.524	$5 < (T - T_c) < 65$	11	318.723285	0.2897	0.9870
2↓	Vert.	742.504	2.822	$2 < (T - T_c) < 95$	19	318.722786	0.3222	0.9589
3↓	Vert.	745.459	3.087	$5 < (T - T_c) < 95$	18	318.722176	0.2225	1.0224
4↓	Vert.	739.828	5.039	$4 < (T - T_c) < 90$	52	318.723464	0.2857	0.9916
5↑	Vert.	740.043	5.039	$2 < (T - T_c) < 89$	46	318.723201	0.2907	0.9897
6↓	Vert.	744.841	4.986	$4 < (T - T_c) < 90$	52	318.723432	0.3083	0.9805
7↑	Vert.	744.939	4.939	$2 < (T - T_c) < 89$	46	318.722923	0.2584	1.0006
8↑	Hor.	742.059	3.332	$10 < (T - T_c) < 90$	33	318.721982	0.3547	0.9560
"	"	"	"	$0 < (T - T_c) < 10$	12	318.722979	0.2217	1.0000
Fig. 2	Vert.			$3 < (T - T_c) < 90$	224	318.723149	0.2804	0.9928

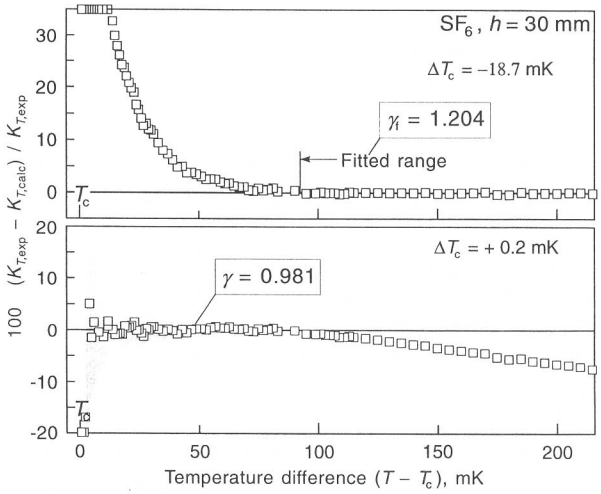

Fig. 4. Percentage deviations of experimental $K_{T,\mathrm{expt}}$ values for sulfur hexafluoride (run 6↓, vertical cells) from values $K_{T,\mathrm{calc}}$ calculated from Eq. (3) fitted to $K_{T,\mathrm{expt}}$ values of the outer temperature range 90 mK $< (T - T_c) <$ 215 mK (upper diagram) and to $K_{T,\mathrm{expt}}$ values of the inner temperature range 4 mK $< (T - T_c)$ $<$ 90 mK (lower diagram). The gray consistency band around the data in the lower diagram, which was calculated for an error of $\Delta(\Delta p) = 0.2$ Pa, also illustrates the fitting range of the corresponding K_T equation.

far above T_c. Nevertheless, the absolute agreement of the differential pressures of run 4↓ and run 5↑ (measured between the isochores filled with ρ_c and $\rho_c - 5\ \mathrm{kg \cdot m^{-3}}$) and of run 6↓ and run 7↑ (measured between the isochores filled with ρ_c and $\rho_c + 5\ \mathrm{kg \cdot m^{-3}}$) is better than ± 0.25 Pa in the near-critical fitting range. Even the visible "great" deviation of the K_T data measured with decreasing temperature from their equivalence measured with increasing temperature in the range $\tau < 1 \times 10^{-5}$ accounts for a difference in differential pressure of only 0.2 Pa. This excellent agreement of the differential pressures (and the corresponding agreement of the isothermal compressibilities), which is so much better than the claimed uncertainty of $\Delta(\Delta p) \leqslant \pm 6$ Pa, is based on the possibility of a zero-point adjustment of the differential pressures just below the saturation line within the quoted consistency of the differential pressure of $\Delta(\Delta p) \leqslant \pm 0.2$ Pa. Based on these facts we believe that the difference between the two slopes is far outside the uncertainty of the measured data for the isothermal compressibility, although it seems quite difficult to give an absolute value for this uncertainty.

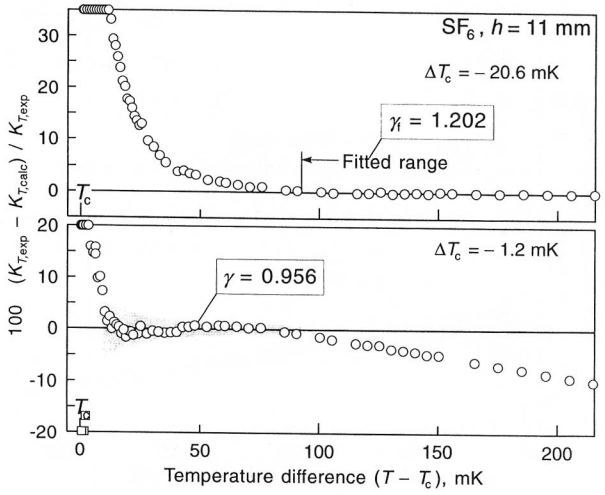

Fig. 5. Percentage deviations of experimental $K_{T,\mathrm{expt}}$ values for sulfur hexafluoride (run 8↑, horizontal cells) from values $K_{T,\mathrm{calc}}$ calculated from Eq. (3) fitted to $K_{T,\mathrm{expt}}$ values of the outer temperature range 95 mK $< (T - T_c) <$ 215 mK (upper diagram) and to $K_{T,\mathrm{expt}}$ values of the inner temperature range 10 mK $< (T - T_c) <$ 90 mK (lower diagram). The gray consistency band around the data in the lower diagram, which was calculated for an error of $\Delta(\Delta p) = 0.2$ Pa, also illustrates the fitting range of the corresponding K_T equation.

The corresponding data for CO_2, as shown in Fig. 3, which includes run 11↓ recorded with decreasing temperature and the equivalent run 12↑ recorded with increasing temperature, are in general a strong confirmation of the results obtained for SF_6. However, due to the position of the vertical cells used for measuring the isothermal compressibility at this time—just beside another DPI used for transmitting the absolute pressure—the scatter of these data is 2.5 times larger. Nevertheless, we also found for CO_2 the same two characteristic slopes and nearly the same values for the critical exponent γ. It should be mentioned that, besides the plotted data and the given numerical values, Fig. 3 is the duplicate of Fig. 2: the slopes shown in Fig. 3 are actually taken from Fig. 2. While in Fig. 2 the line of the near-critical slope was drawn tangentially to the upper border of the data symbols, in Fig. 3 this line taken from Fig. 2 goes along the center of the data symbols. This makes it easier to see that the CO_2 data track the line of the far-critical slope much longer than the SF_6 data do when approaching the critical point.

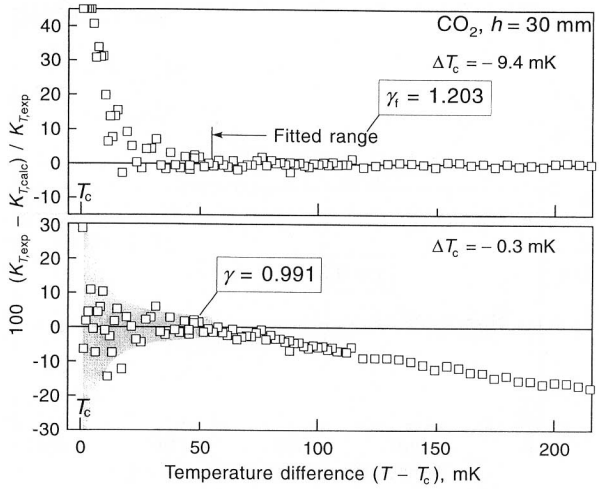

Fig. 6. Percentage deviations of experimental $K_{T,\mathrm{expt}}$ values for carbon dioxide (run 11↓, vertical cells) from values $K_{T,\mathrm{calc}}$ calculated from Eq. (3) fitted to $K_{T,\mathrm{expt}}$ values of the outer temperature range 56 mK $< (T - T_c) <$ 214 mK (upper diagram) and to $K_{T,\mathrm{expt}}$ values of the inner temperature range 1 mK $< (T - T_c) <$ 55 mK (lower diagram). The gray consistency band around the data in the lower diagram, which was calculated for an error of $\Delta(\Delta p) = 0.5$ Pa, also illustrates the fitting range of the corresponding K_T equation.

The two regions for which Eq. (3) yields systematically different values for γ and the position of the transition point between these two regions are shown in some more detail in Figs. 4 to 7 for selected runs of both fluids, run 6↓ and run 8↑ for SF_6 and run 11↑ and run 9↑ for CO_2. In these figures the difference between the true critical temperature of the fluid and the fitted critical temperature according to Eq. (3) is characterized by the value ΔT_c. For both types of measuring cells, vertical and horizontal ones, we found an inner region, where the determined parameter γ in Eq. (3) becomes about 1.0. Beyond a more or less distinct transition point [$(T - T_c) \approx 90$ mK or $\tau \approx 2.82 \times 10^{-4}$ for SF_6 and $(T - T_c) \approx 55$ mK or $\tau \approx 1.81 \times 10^{-4}$ for CO_2], for the outer region the fit yields a value for γ of about 1.2. It should be emphasized that any attempt to fit Eq. (3) simultaneously to K_T data points from the inner and outer temperature region leads to a systematic misrepresentation of the experimental data.

The slightly smaller values of $\gamma = 0.956$ (SF_6) and $\gamma = 0.947$ (CO_2) for the horizontal cells and their deviations from the zero line of the fit near T_c are caused by a very small change in the slope of the data about 10 mK

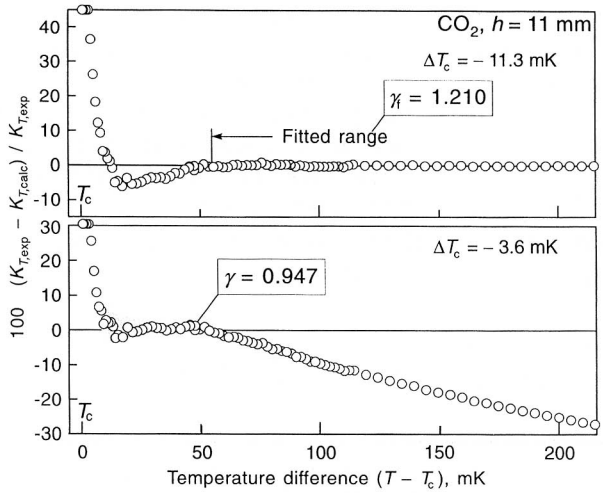

Fig. 7. Percentage deviations of experimental $K_{T,\mathrm{expt}}$ values for carbon dioxide (run 9↓, horizontal cells) from values $K_{T,\mathrm{calc}}$ calculated from Eq. (3) fitted to $K_{T,\mathrm{expt}}$ values of the outer temperature range 56 mK $< (T - T_c) <$ 214 mK (upper diagram) and to $K_{T,\mathrm{expt}}$ values of the inner temperature range 9 mK $< (T - T_c) <$ 55 mK (lower diagram). The gray consistency band around the data in the lower diagram, which was calculated for an error of $\Delta(\Delta p) = 0.2$ Pa, also illustrates the fitting range of the corresponding K_T equation.

Table II. Fitting of Eq. (3) to the Experimental K_T Data for Sulfur Hexafluoride (Outer Region)

Run	Cells	$\bar{\rho}$ (kg·m^{-3})	$\Delta\rho$ (kg·m^{-3})	Temperature range (mK)	Data points	$T_{c,f}$ (K)	$p_c\Gamma$	γ_f
1↓	Vert.	744.311	14.524	$90<(T-T_c)<666$	4	318.705358	0.06238	1.2015
2↓	Vert.	742.504	2.822	$95<(T-T_c)<315$	6	318.694479	0.06149	1.2005
3↓	Vert.	745.459	3.087	$95<(T-T_c)<315$	6	318.702412	0.06180	1.2079
4↓	Vert.	739.828	5.039	$90<(T-T_c)<215$	30	318.704670	0.06006	1.2111
6↓	Vert.	744.841	4.986	$90<(T-T_c)<215$	30	318.704522	0.06173	1.2045
8↑	Hor.	742.059	3.332	$95<(T-T_c)<215$	17	318.702581	0.05935	1.2023
Fig. 2	Vert.			$564<(T-T_c)<3914$	89	318.708826	0.06096	1.2058

above T_c, which restricts the possible fitting range to temperatures above or below this limit. When, however, restricting the fitting range to temperatures $0\leqslant(T-T_c)\leqslant 10$ mK, the values of γ for the horizontal cells meet the values of γ for the vertical cells. The absolute values for the K_T data of the horizontal cells are, however, over the whole temperature range (run 8↑), or only over the near-critical temperature range (run 9↓), slightly lower than for the vertical cells. We argue that these deviations result from a nonperfect correction of the high contributions of the hydrostatic head of the fluid above the horizontally aligned membrane; furthermore, in this case the DPI no longer tends to its zero point when approaching the critical point. In general, we rate the results for the horizontal cells as a strong validation of the essential results obtained with the vertical cells.

We observed these different inner and outer regions for all of our measurements. An overview of the various experimental runs carried out with SF_6 ($\rho_c=742.3$ kg·m^{-3}) and CO_2 ($\rho_c=467.6$ kg·m^{-3}) is given in

Table III. Fitting of Eq. (3) to the Experimental K_T Data for Carbon Dioxide (Inner Region)

Run	Cells	$\bar{\rho}$ (kg·m^{-3})	$\Delta\rho$ (kg·m^{-3})	Temperature range (mK)	Data points	T_c (K)	$p_c\Gamma$	γ
9↓	Hor.	467.569	1.917	$9<(T-T_c)<55$	29	304.132682	0.4884	0.9465
"	"	"	"	$0<(T-T_c)<9$	10	304.136228	0.2598	0.9774
10↑	Hor.	467.592	1.917	$6<(T-T_c)<55$	28	304.132929	0.3469	0.9829
11↓	Vert.	468.511	1.998	$1<(T-T_c)<55$	37	304.135969	0.3236	0.9906
12↑	Vert.	468.504	2.002	$3<(T-T_c)<55$	31	304.137258	0.4433	0.9497
13↓	Vert.	467.714	2.300	$10<(T-T_c)<64$	12	304.134782	0.5943	0.9395
Fig. 3	Vert.			$1<(T-T_c)<55$	70	304.136314	0.3433	0.9821

Table IV. Fitting of Eq. (3) to the Experimental K_T Data for Carbon Dioxide (Outer Region)

Run	Cells	$\bar{\rho}$ (kg·m^{-3})	$\Delta\rho$ (kg·m^{-3})	Temperature range (mK)	Data points	$T_{c,\Gamma}$ (K)	$p_c\Gamma$	γ_Γ
9↓	Hor.	467.569	1.917	$56 < (T - T_c) < 214$	50	304.125002	0.05920	1.2098
10↑	Hor.	467.592	1.917	$56 < (T - T_c) < 214$	46	304.125437	0.06662	1.1920
11↓	Vert.	468.511	1.998	$56 < (T - T_c) < 214$	50	304.126852	0.06212	1.2026
12↑	Vert.	468.504	2.002	$56 < (T - T_c) < 214$	46	304.128650	0.07031	1.1845
13↓	Vert.	467.714	2.300	$56 < (T - T_c) < 214$	22	304.120268	0.07514	1.2123
Fig. 3	Vert.			$313 < (T - T_c) < 2864$	51	304.131066	0.06594	1.1916

Tables I to IV. The numerical values of the experimental data shown in Fig. 4 (run 6↓ of SF_6) and Fig. 6 (run 11↓ of CO_2) are listed in Tables AI and AII in Appendix B. The experimental data of the other runs are available on request from the authors; these data will be published later [6–8]. In Tables II and IV, the values listed for the fitted parameters γ and T_c in Eq. (3) are referred to as γ_Γ and $T_{c,\Gamma}$. They were determined from K_T data measured in the outer, "far-critical" region; these values do not represent the critical parameter γ and the critical temperature T_c. Experimental values for γ and T_c are reported in Tables I and III. Strong evidence that the inner region is the "right" one, which meets the power law within its physical meaning, is given by the values of critical temperature. Thus, the

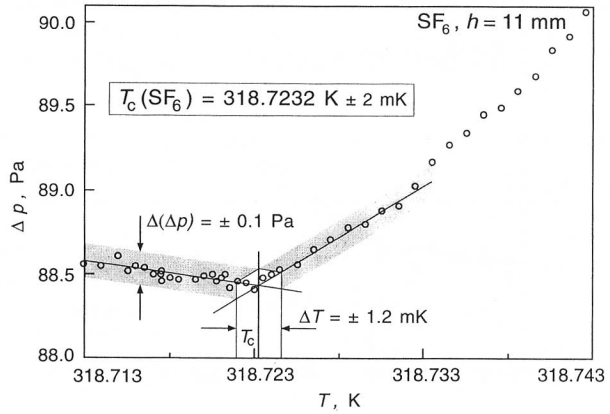

Fig. 8. Differential pressures measured between two near-critical isochores ($\rho_c + 1.625$ kg·m^{-3}, $\rho_c - 1.707$ kg·m^{-3}) with the horizontal cells filled with SF_6, plotted vs absolute temperature.

values for T_c obtained from fitting Eq. (3) to data from the inner region are almost in excellent agreement ($\Delta T_c \leqslant \pm 1.2$ mK) with the critical temperature, which we determined with an independent method as $T_c = 318.7232\ \text{K} \pm 2\ \text{mK}$ for SF_6 and $T_c = 304.1363\ \text{K} \pm 2\ \text{mK}$ for CO_2 [5, 6], as shown in Figs. 8 and 9, respectively.

On the ΔP–T diagram for SF_6 in Fig. 8, we have plotted the differential pressures of run 8↑, measured between the two isochores of the horizontal cells, against the absolute temperature in the immediate vicinity of the critical point. As can be seen by means of the high base level of the differential pressure of about 88.5 Pa (mainly the hydrostatic weight of the fluid above the membrane in this case), these pressures are still uncorrected for the averaging error. Thus, this diagram is not influenced by the critical parameters of the equations of state used for such corrections or any other further evaluations. Due to the sharp discontinuity of the differential pressure, which happens when the two near-critical isochores cross the saturation line, and by means of the apparent consistency of the differential pressure of better than 0.1 Pa, the critical temperature can be determined with an evaluation uncertainty of about 1.2 mK. The corresponding value of the evaluation uncertainty in the case of CO_2 amounts to 1 mK, as shown in Fig. 9 for the differential pressures of run 9↓, and their repetition values, respectively. These repetition values were taken just after crossing the phase boundary during run 9↓ and confirm the very high reproducibility of our measurements above and below the critical point.

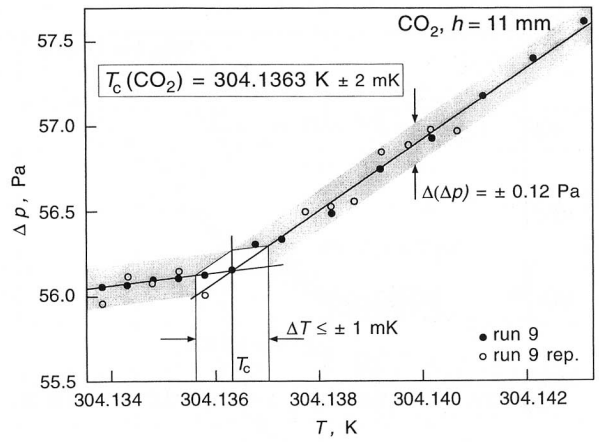

Fig. 9. Differential pressure measured between two near-critical isochores ($\rho_c + 1.917\ \text{kg} \cdot \text{m}^{-3}$, $\rho_c - 1.917\ \text{kg} \cdot \text{m}^{-3}$) with the horizontal cells filled with CO_2, plotted vs absolute temperature.

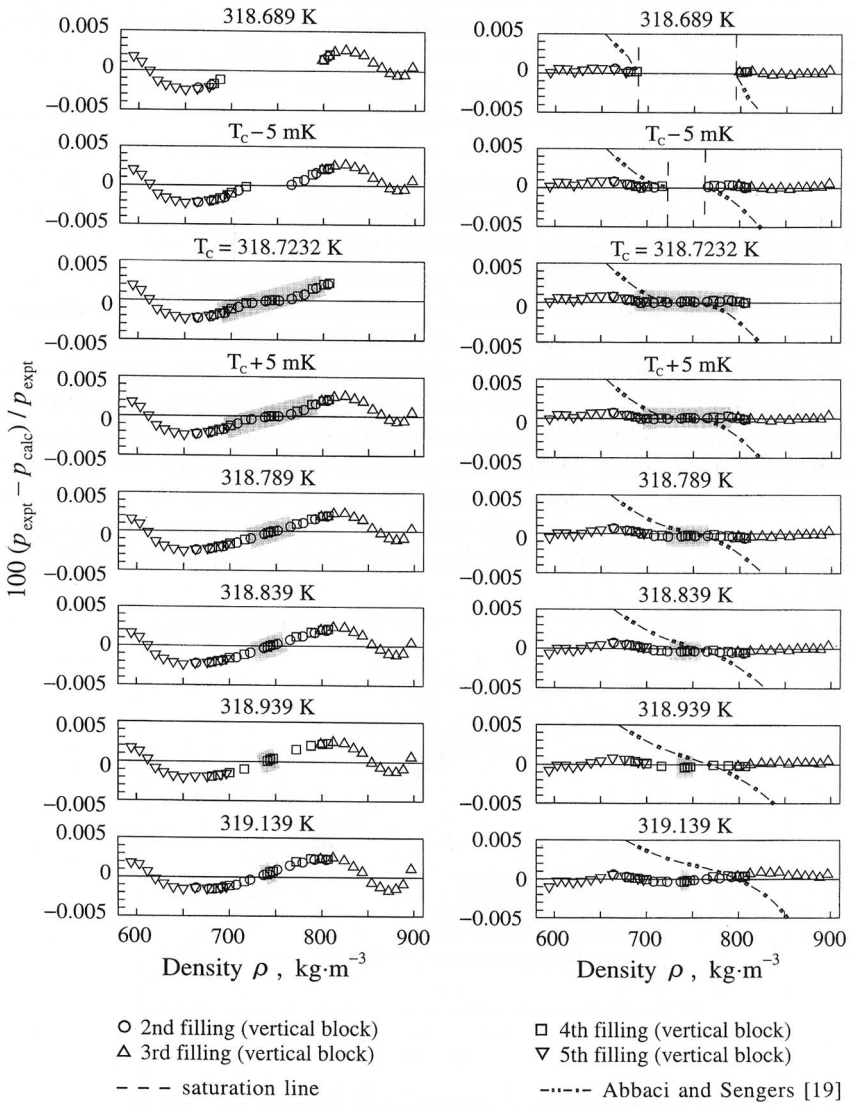

Fig. 10. Relative-pressure deviations of experimental $p\rho T$ values of SF_6 from values p_{calc} calculated from a revised and extended scaling equation (left side) and from an analytical equation of state (right side). These experimental $p\rho T$ values of SF_6 will be published soon. The diagrams on the right side also include the deviations of a crossover equation from the zero line calculated from our analytical equation of state. The shaded area on each isotherm characterizes the variation in density, which corresponds to the calculated density profile over the height of the cells.

While the fitted critical temperatures of the near-critical temperature ranges meet the true critical temperatures almost even within their evaluation uncertainty (except for the horizontal cells of CO_2), the critical temperatures reported by optical measurements [11–16] are even lower than our far-critical temperatures $T_{c,f}$ given in Tables II and IV. On the other hand, the agreement between our critical temperature for SF_6 and the critical temperature reported by Ivanow [17] for their direct $p\rho T$ measurements with extremely pure SF_6 amounts only to 1.5 mK, i.e., the agreement is within our given absolute uncertainty of ± 2 mK.

As given in Appendix A (and reported in Refs. 3 and 5), we developed a mathematical model to correct the averaging error due to the gravity-induced density stratification in the measuring cells (implicit gravity effect). This implies the use of an equation of state which represents the experimental data nearly within their consistency. For carrying out these corrections we developed analytical equations of state for the critical region of SF_6 and CO_2 which meet this requirement. Alternatively, we also used revised and extended scaling equations for such corrections. In this case we used the functional form and the values for the critical exponents given in Ref. 18 and fitted only the coefficients and the critical parameters T_c, ρ_c,

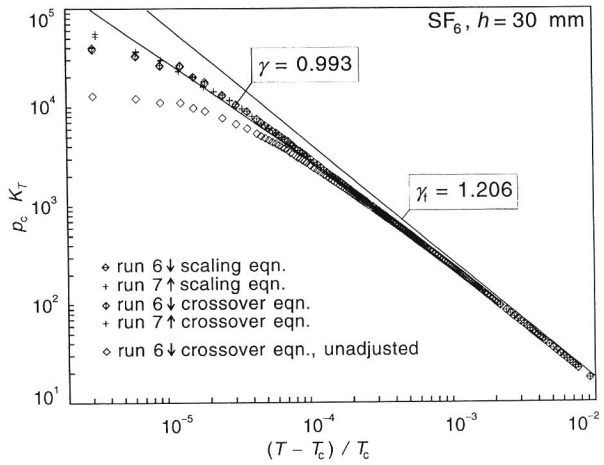

Fig. 11. Dimensionless isothermal compressibility $p_c K_T$ plotted vs the dimensionless temperature difference $(T - T_c)/T_c$ for the K_T data of run 6↓ and run 7↑ of SF_6, which were gravity corrected using nonanalytical equations. The zero point of the DPI was adjusted by $\Delta p = -1.43$ Pa for the use of the crossover equation and by $\Delta p = -1.12$ Pa for the use of the revised and extended scaling equation. Additional information on individual runs is given in Tables I and V.

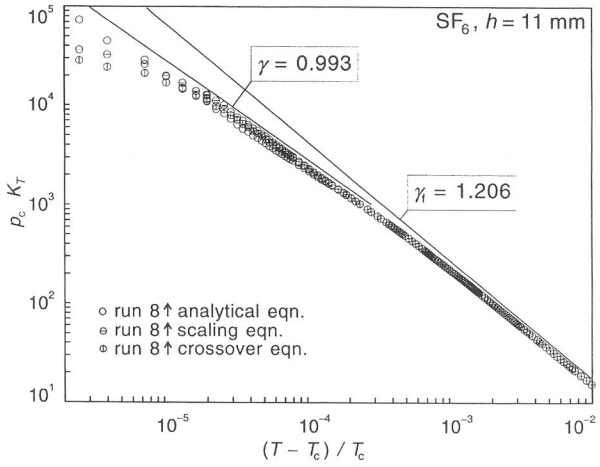

Fig. 12. Dimensionless isothermal compressibility $p_c K_T$ plotted vs the dimensionless temperature difference $(T - T_c)/T_c$ for the K_T data of run 8↑ of SF_6, which were gravity corrected using nonanalytical equations. Additional information is given in Tables I and V.

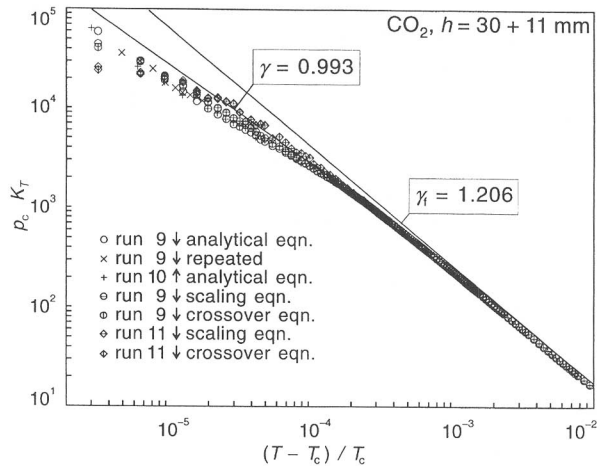

Fig. 13. Dimensionless isothermal compressibility $p_c K_T$ plotted vs the dimensionless temperature difference $(T - T_c)/T_c$ for the K_T data of run 9↓, run 10↑, and run 11↓ of CO_2, which were gravity corrected using nonanalytical equations. Additional information on individual runs is given in Tables III and VI.

and p_c of these equations to our ppT data. Additionally, we used crossover equations [19, 20], which were not fitted to our data but were used by us with our values for the critical parameters. Although these types of equations do not represent our data as well as the analytical equations (see Fig. 10 for SF_6 and Ref. 5 for CO_2), the determined values of the critical exponent γ are in the range between 0.94 and 1.12. Selected runs of both fluids, which were gravity-corrected with nonanalytical equations, are shown in Figs. 11 to 13. As done previously in the case of Fig. 3 and in order to give a standard of comparison, the two slopes shown in each diagram were again taken from Fig. 2. The corresponding values of the fitting parameters are given in Table V for SF_6 and Table VI for CO_2.

As expected, we found the greatest influence of the nonanalytical equations for SF_6 at a cell height of 30 mm, as shown in Fig. 11. Due to the strong gravity influence, however, we had to correct the zero point of the DPI. When using the zero point of the DPI determined in the two-phase region with the help of an analytical equation, we obtained near-critical K_T data nearly independent of the difference $(T-T_c)/T_c$, and too low values for the fitted critical temperature (see the diamond symbols in Fig. 11). When, however, adjusting the zero point of the DPI in such a manner that the fitted critical temperature of the fitting range as close as possible to the critical temperature $[10^{-5} \leqslant (T-T_c)/T_c \leqslant 7 \times 10^{-5}]$ meets the true critical temperature of SF_6, then the values for the critical exponent γ remain with $\gamma = 1.059$ (crossover equation) and $\gamma = 1.077$ (revised and extended scaling equation) close to the classical value. It should be mentioned that this fitting range is quite comparable with the fitting ranges, which were achieved in those optical experiments closest to the critical point (see Refs. 15 and 16).

Table V. Fitting of Eq. (3) to Selected Experimental K_T Data for Sulfur Hexafluoride that Were Gravity Corrected Using Nonanalytical Equations (Inner Region Only)[a]

Run	Cells	Type of equation	Temperature range (mK)	Data points	T_c (K)	$p_c\Gamma$	γ
6↓	Vert.	Crossover	$4 < (T-T_c) < 23$	17	318.723216	0.1875	1.0592
"	"	"	$8 < (T-T_c) < 90$	49	318.723364	0.1171	1.1059
7↑	Vert.	Crossover	$13 < (T-T_c) < 89$	38	318.723354	0.1090	1.1125
8↑	Hor.	Crossover	$6 < (T-T_c) < 90$	38	318.723426	0.3047	0.9725
6↓	Vert.	Scaling	$4 < (T-T_c) < 23$	17	318.723134	0.1592	1.0772
"	"	"	$6 < (T-T_c) < 90$	50	318.723316	0.1080	1.1150
7↑	Vert.	Scaling	$13 < (T-T_c) < 89$	38	318.723394	0.1032	1.1185
8↑	Hor.	Scaling	$6 < (T-T_c) < 90$	38	318.724170	0.2934	0.9762

[a] The zero point of the differential pressures of runs 6↓ and 7↑ were adjusted by $\Delta p = -1.43$ Pa for the crossover equation and by $\Delta p = -1.12$ Pa for the scaling equation.

Table VI. Fitting of Eq. (3) to Selected Experimental K_T Data for Carbon Dioxide that Were Gravity Corrected Using Nonanalytical Equations (Inner Region Only)

Run	Cells	Type of equation	Temperature range (mK)	Data points	T_c (K)	$p_c\Gamma$	γ
9↓	Hor.	Crossover	$2<(T-T_c)<17$	15	304.135700	0.3294	0.9748
"	"	"	$17<(T-T_c)<55$	22	304.132050	0.3243	0.9954
10↓	Vert.	Crossover	$7<(T-T_c)<55$	31	304.133797	0.1131	1.1181
9↓	Hor.	Scaling	$2<(T-T_c)<17$	15	304.135724	0.2890	0.9885
"	"	"	$17<(T-T_c)<55$	22	304.132680	0.3618	0.9815
10↓	Vert.	Scaling	$7<(T-T_c)<55$	31	304.134124	0.1159	1.1146

Apparently no shift of the zero point of the DPI will be able to prevent the bending-off of the near-critical data from the far-critical slope, hence this bending-off seems to be a genuine property of our K_T data themselves.

For the horizontal cells with a height of 11 mm the influence of the gravity corrections by means of nonanalytical equations is considerably smaller (see Fig. 12). Without any additional shift of the zero point of the DPI, the values for the critical exponent and the difference of the fitted critical temperature remain for the crossover equation ($\gamma = 0.973$ and $\Delta T_c = 0.2$ mK) and for the revised and extended scaling equation ($\gamma = 0.976$ and $\Delta T_c = 1$ mK) very close to the values obtained when using an analytical equation for the gravity corrections.

As shown in Fig. 13, these results for SF_6 are confirmed by our results for CO_2 obtained with nonanalytical equations for the gravity-induced corrections. Once more we found, for a cell height of 30 mm (run 11↓) with $\gamma = 1.118$ (crossover equation) and $\gamma = 1.115$ (revised and extended scaling equation), slightly higher values for the critical exponent γ; thus, also for CO_2 the values remain closer to the classical than to the nonclassical prediction. For a cell height of 11 mm (run 9↓) the values obtained in the fitting ranges closest to the critical point are, with $\gamma = 0.975$ (crossover equation) and $\gamma = 0.989$ (revised and extended scaling equation), again close to the classical value.

These tests clearly show that the type of equation of state used for these gravity-induced corrections, or the averaging of the K_T data over our finite sample height of 30 and 11 mm, is definitely not responsible for our almost classical values for γ. According to the values given in Figs. 2 and 3, we state these values as

$$\gamma = 0.99 \pm 0.05 \qquad \text{for } SF_6 \tag{4}$$

$$\gamma = 0.98 \pm 0.05 \qquad \text{for } CO_2 \tag{5}$$

We emphasize that for the inner region the averaging error and its correction for horizontal and vertical cells differ in type and size. Since we obtained nearly identical results for the critical exponent γ, we exclude an error in the mathematical model or in computation which is significant for the considerations given above. When determining the parameter γ_f of the outer region ($\gamma_f = 1.206 \pm 0.03$ for SF_6, $\gamma_f = 1.192 \pm 0.03$ for CO_2), the equation of state has no impact, since for the temperature range $(1 \text{ to } 2) \times 10^{-3} < \tau < 1 \times 10^{-2}$, the influence of the averaging error becomes smaller than the statistical error of the corrections. Also for this range it seems remarkable to us that these far-critical values are considerably lower than predicted by the renormalization-group theory. No tendency to higher values of the critical exponent γ seems to be detectable up to the lower limit of this region, as should be expected due to the common corrections to scaling.

The new results are in clear contradiction to the predictions of the renormalization-group theory if pure fluids under gravity in the immediate vicinity of the critical point are considered. An application of the renormalization-group theory which would take into account the influence of gravity as a dominant outer field could perhaps close the gap between the new experimental results and theory. Our experimental results are also in contrast to most measurements reported by other authors [11–16]. However, our measurements were performed with the smallest temperature gradients and the highest purity of fluid ever reported. More than this, in contrast to optical experiments, our experimental K_T values are *directly* based on measured differential pressures and densities according to Eq. (1), and do not depend on the Lorentz–Lorenz relation, which is unproven in the gravity-influenced critical region. Notably, there is a certain agreement when comparing our results with the experiments of Ivanov [17] and Makarevich et al. [21], who performed direct measurements with extremely pure SF_6 and also found two regions of different fluid behavior.

As a result of our measurements we believe that in the immediate vicinity of the critical point, pure fluids under gravity show a universal but nearly classical-like behavior. Apparently in this region the fluid behavior is governed by an explicit gravity effect, which was not expected to be so strong (see Refs. 22 and 23). In an outer region where gravity-induced density stratification does not play any significant part, the behavior of pure fluids is approximately described by the renormalization-group theory. The change between the two kinds of universal behavior in the case of pure fluids occurs at a transition point which seems to depend on the gravity impact on the fluid as indicated by the relation for the two fluids considered here,

$$\tau_{\text{trans.point}}(CO_2)/\tau_{\text{trans.point}}(SF_6) \approx \rho_c(CO_2)/\rho_c(SF_6) \approx 2/3$$

APPENDIX A. CORRECTION OF THE IMPLICIT GRAVITY EFFECT (AVERAGING ERROR)

Due to gravity the measured differential pressures between the two cells are distorted when measuring closely to the critical point. The explanation of this gravity influence exerted on these measurements is given with the help of the left part of Fig. 1. The figure shows schematically two vertical measuring cells, with the differential pressure indicator (DPI) installed between the cells. Provided that the temperature corresponds exactly to the critical temperature and the average densities in the two cells symmetrically surround the critical density, the calculated density profiles over their cell height look like those illustrated. The average density in the left cell is slightly below, and that in the right cell slightly above, the middle of the cells. The height of the measuring cells is $2r$; r_s refers to the radius of the sensitive area A_s of the DPIs.

The differential pressure $(\Delta p)_{DPI}$ indicated by the DPI corresponds to the integrally effecting pressure difference over the membrane of the DPIs; the integral effect depends on the shape of the density stratification. We do not, however, need the indicated value $(\Delta p)_{DPI}$ but the pressure difference $(\Delta p)_{corr}$ between the unknown loci in the two cells where the actual density (of the stratification curves) corresponds exactly to the average density, which is known only from filling. To convert the measured differential pressure $(\Delta p)_{DPI}$ to the wanted value $(\Delta p)_{corr}$, a special mathematical model was developed [3, 5], which is described by the equation

$$\begin{aligned}(\Delta p)_{corr} &= p(\bar{\rho}_H) - p(\bar{\rho}_L) \\ &= (\Delta p)_{DPI} + -\frac{1}{A_s}\left[\int_{-r_s}^{+r_s} (p(z) - p(\bar{z})\, b(z)\, dz)\right]_H \\ &\quad + \frac{1}{A_s}\left[\int_{-r_s}^{+r_s} (p(z) - p(\bar{z})\, b(z)\, dz)\right]_L \end{aligned} \tag{A1}$$

where

H = measuring cell "High" with the higher pressure

L = measuring cell "Low" with the lower pressure

$A_s = \pi r_s^2$ = sensitive area of the membrane of the DPI with the sensitive radius r_s

z = height coordinate of the cell

$\bar{z}$ = height, where the actual density ρ is equal to the average density $\bar{\rho}$

$b(z)$ = width of the measuring cell at height z
(secant of the circular cross section of the measuring cell)

$p(z)$ = pressure in the measuring cell at height z

The function $p(z)$ is calculated from the equation

$$p(z) = p(\bar{z}) - \int_{z(\bar{\rho})}^{z} \rho(z)\, g\, dz \tag{A2}$$

where

$z(\bar{\rho}) = \bar{z}$; see Eq. (A1)

$\rho(z)$ = actual density at height z due to density stratification

For the differential pressure between two horizontal measuring cells, a similar correction has to be made. The right part of Fig. 1 illustrates the correction for two cells which are symmetrically filled around the critical density. Again, the loci of the average density are slightly below and above the middle of the cells, respectively. The differential pressure measured by the DPI is the pressure difference between the two cell membranes, each covered with fluid of a constant pressure. The differential pressure $(\Delta p)_{\text{corr}}$ between the two loci of average density is given by the equation

$$\begin{aligned}(\Delta p)_{\text{corr}} &= p(\bar{\rho}_{\text{H}}) - p(\bar{\rho}_{\text{L}}) \\ &= (\Delta p)_{\text{DPI}} - [\,p(\rho^*) - p(\bar{\rho})\,]_{\text{H}} + [\,p(\rho^*) - p(\bar{\rho})\,]_{\text{L}}\end{aligned} \tag{A3}$$

where

ρ^* = actual density at the bottom (H) or the top (L) of the cell
due to density stratification

Thus, the wanted pressure difference $(\Delta p)_{\text{corr}}$ between either two vertical or two horizontal cells can be calculated from the measured differential pressure $(\Delta p)_{\text{DPI}}$ with the help of Eqs. (A1) to (A3). The numerical evaluation of all the integrals and of the actual density at the bottom and the top of the cell can be carried out using a convenient equation of state. When performing these calculations it turned out that for SF_6 and CO_2 the contributions of the correction for the averaging error exceed the statistical error (0.02 Pa) of these calculations only in a region closer to the critical point than about $\tau \leqslant (1 \text{ to } 2) \times 10^{-3}$.

For these calculations the condition that the correlation length is much smaller than the geometrical dimensions of the system (30 and 11 mm) has to be met. However, even at a distance of 1 mK to the critical point, the correlation length amounts to 0.44 μm for SF_6, [11] and 0.53 μm for CO_2 [12], so this condition is clearly fulfilled.

APPENDIX B. VALUES OF ISOTHERMAL COMPRESSIBILITY

Table AI. Experimental Data for the Isothermal Compressibility of Sulfur Hexafluoride (Run 6↓) for an Average Density of 744.841 kg · m^{-3}, Where T is the Temperature (ITS-90), $\Delta\rho$ the Difference in Density Between the two Isochores, $(\Delta p)_{DPI}$ the Indicated Differential Pressure, $(\Delta p)_{corr}$ the Differential Pressure Corrected for the Implicit Gravity Effect, p_c the Critical Pressure (3.754983 MPa), and K_T the Gravity-Corrected Isothermal Compressibility

T (K)	$\Delta\rho$ (kg · m^{-3})	$(\Delta p)_{DPI}$ (Pa)	$(\Delta p)_{corr}$ (Pa)	$p_c K_T$
323.136908	5.31956	2537.869	2537.864	10.5679
322.637105	5.28018	2182.687	2182.684	12.1968
322.137269	5.23998	1839.526	1839.524	14.3621
321.637407	5.20001	1511.363	1511.370	17.3474
321.137588	5.15992	1197.481	1197.481	21.7260
321.037537	5.15191	1137.303	1137.306	22.8401
320.937551	5.14376	1076.984	1076.963	24.0817
320.837636	5.13553	1017.285	1017.291	25.4535
320.737576	5.12789	958.877	958.850	26.9648
320.637620	5.11960	900.688	900.668	28.6603
320.537587	5.11181	843.839	843.831	30.5443
320.437620	5.10403	787.611	787.622	32.6742
320.337642	5.09600	731.703	731.690	35.1167
320.237652	5.08836	677.064	677.051	37.8938
320.137648	5.08043	623.455	623.451	41.0875
320.087719	5.07680	597.026	597.015	42.8762
320.037695	5.07282	570.396	570.390	44.8424
319.987744	5.06886	544.136	544.138	46.9691
319.937741	5.06508	518.238	518.219	49.2815
319.887789	5.06136	493.028	493.024	51.7619
319.837775	5.05753	467.319	467.303	54.5695
319.787775	5.05380	441.969	441.945	57.6581
319.737739	5.05006	417.420	417.419	61.0006
319.687871	5.04634	392.841	392.815	64.7737
319.637943	5.04277	368.371	368.348	69.0271
319.587916	5.03913	344.561	344.524	73.7473
319.537972	5.03541	320.802	320.755	79.1535
319.487906	5.03182	297.533	297.484	85.2847
319.416938	5.02694	265.073	265.022	95.6380

Table AI. *(Continued)*

T (K)	$\Delta\rho$ (kg · m^{-3})	$(\Delta p)_{DPI}$ (Pa)	$(\Delta p)_{corr}$ (Pa)	$p_c K_T$
319.412955	5.02664	263.193	263.147	96.3137
319.387958	5.02483	251.863	251.820	100.6094
319.362962	5.02313	240.754	240.691	105.2258
319.337902	5.02139	229.544	229.487	110.3245
319.312906	5.01972	218.494	218.445	115.8629
319.287919	5.01804	207.675	207.626	121.8589
319.267849	5.01662	199.026	198.947	127.1391
319.247942	5.01532	190.465	190.420	132.7976
319.237991	5.01464	186.235	186.164	135.8152
319.217836	5.01333	177.786	177.731	142.2223
319.207920	5.01268	173.525	173.446	145.7166
319.197943	5.01203	169.466	169.363	149.2100
319.187968	5.01134	165.226	165.131	153.0124
319.177996	5.01066	160.986	160.897	157.0179
319.167959	5.01006	156.966	156.884	161.0150
319.157967	5.00944	152.876	152.771	165.3290
319.147978	5.00870	148.796	148.695	169.8358
319.137949	5.00813	144.706	144.611	174.6118
319.127966	5.00749	140.727	140.634	179.5265
319.117923	5.00683	136.657	136.540	184.8854
319.107958	5.00624	132.586	132.446	190.5770
319.098019	5.00561	128.587	128.448	196.4843
319.087975	5.00492	124.747	124.602	202.5204
319.078015	5.00434	120.807	120.659	209.1142
319.067914	5.00370	116.828	116.676	216.2253
319.057998	5.00311	113.017	112.858	223.5130
319.047976	5.00245	109.318	109.151	231.0738
319.037988	5.00185	105.378	105.199	239.7248
319.027997	5.00125	101.527	101.365	248.7626
319.017933	5.00064	97.748	97.567	258.4145
319.008049	5.00006	93.978	93.776	268.8294
318.997997	4.99945	90.377	90.148	279.6140
318.988010	4.99890	86.618	86.409	291.6804
318.977999	4.99833	82.898	82.652	304.9039
318.967964	4.99770	79.298	79.030	318.8378
318.958011	4.99710	75.738	75.441	333.9647
318.947973	4.99651	72.208	71.904	350.3514
318.937998	4.99600	68.628	68.302	368.7888
318.933028	4.99572	66.799	66.456	379.0121
318.928051	4.99546	65.079	64.714	389.1941
318.923018	4.99514	63.388	63.025	399.5972

Table AI. *(Continued)*

T (K)	$\Delta\rho$ (kg · m^{-3})	$(\Delta p)_{\mathrm{DPI}}$ (Pa)	$(\Delta p)_{\mathrm{corr}}$ (Pa)	$p_c K_T$
318.917963	4.99489	61.648	61.260	411.0899
318.913025	4.99455	59.979	59.600	422.5105
318.908034	4.99426	58.209	57.765	435.9058
318.902979	4.99402	56.699	56.281	447.3782
318.897983	4.99374	55.008	54.543	461.6058
318.893001	4.99351	53.108	52.619	478.4630
318.888027	4.99319	51.549	51.026	493.3685
318.883009	4.99292	49.899	49.360	509.9913
318.877936	4.99267	48.279	47.708	527.6242
318.873045	4.99244	46.679	46.093	546.0862
318.867977	4.99213	44.999	44.351	567.4978
318.863020	4.99186	43.449	42.775	588.3754
318.858026	4.99163	41.869	41.148	611.6099
318.853013	4.99134	40.309	39.539	636.4613
318.848013	4.99113	38.759	37.921	663.5881
318.842949	4.99087	37.179	36.307	693.0510
318.838016	4.99063	35.699	34.760	723.8598
318.836019	4.99053	35.059	34.100	737.8530
318.834007	4.99029	34.540	33.562	749.6451
318.832031	4.99036	34.009	32.985	762.7686
318.830021	4.99024	33.340	32.285	779.2858
318.828013	4.99012	32.729	31.658	794.7004
318.826064	4.99003	32.159	31.067	809.8050
318.824037	4.98992	31.539	30.392	827.7697
318.821947	4.98983	30.990	29.807	843.9994
318.817908	4.98964	29.849	28.587	879.9822
318.813122	4.98952	28.369	26.998	931.7523
318.806005	4.98907	26.459	24.919	1009.3941
318.804126	4.98911	25.820	24.209	1039.0065
318.802006	4.98887	25.320	23.649	1063.5594
318.800037	4.98887	24.839	23.113	1088.2229
318.798006	4.98868	24.239	22.436	1121.0125
318.795904	4.98857	23.829	21.948	1145.9128
318.793934	4.98853	23.269	21.335	1178.8281
318.791996	4.98839	22.680	20.659	1217.3630
318.789994	4.98833	22.219	20.097	1251.3920
318.787853	4.98826	21.640	19.451	1292.9288
318.785867	4.98824	21.060	18.786	1338.6929
318.784096	4.98817	20.700	18.316	1373.0249
318.782127	4.98804	20.179	17.716	1419.4895
318.780109	4.98790	19.669	17.071	1473.0755

Table AI. *(Continued)*

T (K)	$\Delta\rho$ (kg · m^{-3})	$(\Delta p)_{\mathrm{DPI}}$ (Pa)	$(\Delta p)_{\mathrm{corr}}$ (Pa)	$p_c K_T$
318.778095	4.98788	19.210	16.517	1522.4780
318.776129	4.98778	18.800	16.001	1571.5368
318.774148	4.98770	18.300	15.381	1634.8584
318.772056	4.98760	17.830	14.760	1703.6110
318.770077	4.98758	17.409	14.191	1771.9039
318.768018	4.98749	17.009	13.661	1840.6146
318.766153	4.98739	16.529	13.016	1931.7804
318.764125	4.98734	16.180	12.521	2008.1312
318.762169	4.98728	15.690	11.853	2121.2791
318.760152	4.98719	15.230	11.216	2241.7060
318.758160	4.98713	14.880	10.657	2359.2607
318.756154	4.98705	14.419	10.016	2510.2095
318.754182	4.98701	13.969	9.368	2683.8113
318.753141	4.98697	13.790	9.075	2770.4427
318.752156	4.98696	13.649	8.827	2848.2730
318.751123	4.98687	13.430	8.494	2959.8764
318.750058	4.98688	13.360	8.298	3029.7914
318.749108	4.98679	13.120	7.958	3159.1712
318.748085	4.98673	12.899	7.592	3311.4333
318.747071	4.98676	12.720	7.300	3443.9090
318.746183	4.98670	12.440	6.919	3633.5045
318.745055	4.98667	12.300	6.627	3793.5745
318.744080	4.98666	12.170	6.352	3957.7982
318.743083	4.98662	11.990	6.062	4147.1041
318.742171	4.98659	11.810	5.765	4360.7123
318.741126	4.98656	11.719	5.536	4541.0663
318.740134	4.98651	11.549	5.221	4814.9867
318.739140	4.98649	11.390	4.924	5105.3881
318.738138	4.98643	11.240	4.621	5440.0832
318.737164	4.98643	11.040	4.280	5873.5119
318.735146	4.98637	10.690	3.628	6928.9477
318.735161	4.98642	10.670	3.608	6967.4347
318.733185	4.98635	10.470	3.104	8098.6217
318.731208	4.98631	10.129	2.454	10243.6125
318.729246	4.98628	9.810	1.818	13827.1031
318.728224	4.98623	9.700	1.551	16207.2579
318.727277	4.98624	9.489	1.167	21540.2165
318.726135	4.98618	9.530	1.020	24644.2203
318.725190	4.98617	9.399	0.720	34912.5000
318.724185	4.98615	9.310	0.460	54645.4151
318.723103	4.98613	9.120	0.073	344338.101

Table AII. Experimental Data for the Isothermal Compressibility of Carbon Dioxide (Run 11↓) for an Average Density of 468.511 $kg \cdot m^{-3}$, Where T is the Temperature (*ITS-90*), $\Delta\rho$ the Difference in Density Between the two Isochores, $(\Delta p)_{DPI}$ the Indicated Differential Pressure, $(\Delta p)_{corr}$ the Differential Pressure Corrected for the Implicit Gravity Effect, p_c the Critical Pressure (7.378491 MPa), and K_T the Gravity-Corrected Isothermal Compressibility

T (K)	$\Delta\rho$ ($kg \cdot m^{-3}$)	$(\Delta p)_{DPI}$ (Pa)	$(\Delta p)_{corr}$ (Pa)	$p_c K_T$
310.000267	1.53675	3272.28	3272.288	7.3974
307.500198	1.72850	1921.78	1921.794	14.1662
307.250248	1.74181	1768.11	1768.104	15.5158
307.000241	1.76975	1628.23	1628.229	17.1190
306.750181	1.79049	1479.01	1479.014	19.0668
306.500210	1.82230	1336.53	1336.522	21.4746
306.400266	1.81573	1265.12	1265.114	22.6044
306.300243	1.82187	1203.27	1203.290	23.8460
306.200186	1.84009	1150.24	1150.240	25.1955
306.100200	1.85730	1094.32	1094.323	26.7309
306.000180	1.85336	1026.91	1026.896	28.4251
305.900204	1.86993	970.72	970.719	30.3391
305.800189	1.86739	903.39	903.392	32.5554
305.700208	1.89794	853.29	853.295	35.0313
305.600206	1.88099	779.31	779.324	38.0127
305.500229	1.88753	721.65	721.668	41.1921
305.400233	1.89001	659.33	659.328	45.1456
305.300226	1.91515	606.54	606.541	49.7281
305.200212	1.92341	547.17	547.176	55.3609
305.150198	1.92884	518.47	518.458	58.5923
305.100215	1.93152	488.90	488.917	62.2188
305.050232	1.92931	457.25	457.268	66.4484
305.000255	1.91920	426.20	426.220	70.9142
304.950237	1.94199	401.46	401.460	76.1833
304.900226	1.95211	374.65	374.653	82.0602
304.850231	1.95363	346.57	346.565	88.7794
304.825215	1.94990	331.26	331.257	92.7042
304.800087	1.95911	318.66	318.658	96.8255
304.775112	1.94979	303.65	303.650	101.1263
304.750087	1.96408	291.73	291.713	106.0371
304.725117	1.96856	278.29	278.272	111.4130
304.700095	1.97494	265.15	265.137	117.3118
304.674304	1.95846	248.28	248.269	124.2338
304.649262	1.96720	236.35	236.342	131.0865
304.624309	1.96726	222.50	222.493	139.2503
304.609281	1.98053	216.30	216.295	144.2083
304.599296	1.97764	210.32	210.316	148.0910
304.589322	1.96422	203.99	203.966	151.6632
304.579295	1.96412	198.15	198.148	156.1076

Table AII. *(Continued)*

T (K)	$\Delta\rho$ (kg · m^{-3})	$(\Delta p)_{DPI}$ (Pa)	$(\Delta p)_{corr}$ (Pa)	$p_c K_T$
304.569306	1.97555	193.93	193.909	160.4509
304.559299	1.97646	189.23	189.211	164.5104
304.549311	1.96489	182.64	182.630	169.4382
304.539332	1.96880	177.34	177.322	174.8580
304.529306	1.96759	171.98	171.963	180.1960
304.519293	1.96626	167.27	167.255	185.1424
304.509282	1.99421	164.25	164.236	191.2323
304.499291	1.98740	159.36	159.347	196.4248
304.489259	1.98213	153.81	153.776	202.9991
304.489386	1.98206	153.35	153.338	203.5717
304.479409	1.98190	147.85	147.818	211.1563
304.469402	1.97991	142.87	142.861	218.2639
304.459474	1.95841	135.85	135.843	227.0420
304.449451	1.97154	132.87	132.844	233.7269
304.439423	1.97883	127.60	127.575	244.2812
304.429397	1.98795	123.81	123.788	252.9166
304.419372	1.99183	119.42	119.385	262.7579
304.409391	1.97842	113.66	113.627	274.2101
304.399357	1.98846	108.78	108.750	287.9644
304.389428	1.96968	103.42	103.412	299.9614
304.379429	1.97590	98.48	98.455	316.0613
304.369481	1.97850	93.29	93.249	334.1463
304.359437	1.98613	89.88	89.832	348.1969
304.349430	1.98337	85.25	85.232	366.4776
304.344430	1.97241	82.30	82.258	377.6234
304.339417	1.98280	80.27	80.253	389.1010
304.334438	1.96403	77.45	77.412	399.5592
304.329395	1.98999	76.88	76.844	407.8404
304.324383	1.97672	73.77	73.735	422.1953
304.319357	1.99584	72.46	72.405	434.1191
304.314369	1.99194	69.53	69.499	451.3853
304.309363	1.97598	67.42	67.370	461.9097
304.304416	1.97229	64.53	64.482	481.6954
304.299368	1.99688	63.33	63.266	497.0866
304.294424	1.97194	59.98	59.919	518.2844
304.289439	1.98127	58.04	57.981	538.1484
304.284374	1.98893	56.91	56.862	550.8643
304.279418	1.97663	54.06	53.989	576.5807
304.274405	1.98269	51.89	51.823	602.5268
304.269404	1.99062	49.91	49.847	628.9210
304.264401	1.99692	48.10	48.017	654.9616
304.259397	1.99612	46.26	46.160	681.0368
304.254371	2.00744	44.65	44.556	709.5608

Table AII. *(Continued)*

T (K)	$\Delta\rho$ (kg m^{-3})	$(\Delta p)_{DPI}$ (Pa)	$(\Delta p)_{corr}$ (Pa)	$p_c K_T$
304.249418	1.97812	40.97	40.861	762.4032
304.247413	1.98084	40.85	40.764	765.2703
304.245403	1.99694	40.38	40.257	781.2181
304.243380	1.99832	39.63	39.529	796.1580
304.241394	1.98937	38.36	38.244	819.2147
304.239384	1.99868	38.06	37.930	829.8694
304.237395	2.00005	37.02	36.894	853.7575
304.235384	1.99569	36.31	36.187	868.5357
304.233392	1.99485	35.42	35.278	890.5424
304.231376	1.99707	34.99	34.873	901.8897
304.229385	1.99234	33.99	33.856	926.7742
304.227410	1.98471	32.85	32.699	955.8865
304.225397	1.98762	32.25	32.084	975.6406
304.223399	1.99436	31.41	31.248	1005.1458
304.223402	2.00682	32.52	32.358	976.7438
304.221404	2.00257	30.95	30.793	1024.2030
304.219408	1.98664	29.75	29.579	1057.7399
304.217432	1.98048	28.98	28.807	1082.7105
304.215423	1.99452	28.20	28.004	1121.6702
304.213421	1.97999	27.63	27.452	1135.8695
304.211441	1.99062	26.38	26.182	1197.3758
304.209327	1.98463	25.78	25.588	1221.4755
304.207300	1.99096	25.46	25.227	1242.9146
304.205301	1.98898	24.68	24.455	1280.8761
304.203277	2.00471	24.26	24.020	1314.4060
304.201259	2.00072	23.68	23.426	1345.0452
304.199442	1.97239	22.09	21.823	1423.3590
304.197315	1.98873	21.92	21.642	1447.1807
304.195314	2.00760	21.28	20.972	1507.6124
304.193332	1.99170	20.13	19.815	1582.9820
304.191307	2.00496	19.87	19.529	1616.8775
304.189296	1.99652	18.93	18.576	1692.6566
304.187295	1.99555	18.42	18.037	1742.3914
304.185305	2.00575	17.34	16.931	1865.7170
304.183320	1.98220	16.39	15.959	1956.0590
304.181300	1.97936	16.38	15.911	1959.1441
304.183315	1.99377	16.63	16.199	1938.3518
304.181273	1.99543	16.31	15.842	1983.6861
304.179329	1.98779	15.23	14.725	2125.9746
304.177304	1.99903	15.14	14.593	2157.3623
304.175300	2.00078	14.40	13.797	2283.8269
304.173319	1.98297	13.19	12.538	2490.7381
304.171313	1.98375	13.16	12.473	2504.7093

Table AII. *(Continued)*

T (K)	$\Delta\rho$ (kg·m^{-3})	$(\Delta p)_{DPI}$ (Pa)	$(\Delta p)_{corr}$ (Pa)	$p_c K_T$
304.169287	1.99207	12.48	11.728	2675.0138
304.167328	1.99312	11.10	10.251	3062.0565
304.165304	1.99484	10.85	9.923	3166.0022
304.163304	1.99295	10.34	9.307	3372.3386
304.161306	1.99671	10.37	9.223	3409.4896
304.159294	2.00033	9.74	8.451	3727.7062
304.157295	1.99227	8.86	7.426	4225.1070
304.155304	1.99611	8.18	6.567	4787.0039
304.153283	2.00445	8.63	6.826	4624.6660
304.151307	1.98417	7.06	5.065	6169.3505
304.150315	1.99062	7.05	4.930	6358.9419
304.149275	2.00571	7.31	5.038	6269.8953
304.148284	1.99672	6.84	4.440	7082.4148
304.147278	1.99651	7.09	4.545	6918.0565
304.146293	1.99986	6.35	3.674	8572.5473
304.145344	1.97500	5.74	2.931	10611.7818
304.144331	1.98197	5.74	2.757	11321.3913
304.143314	1.99439	5.65	2.475	12690.5667
304.142301	1.99065	5.72	2.395	13089.8107
304.141311	1.98984	5.43	1.894	16545.6006
304.140305	1.99201	5.08	1.368	22932.4069
304.139278	1.99964	5.04	1.127	27943.1914
304.138314	1.99053	4.91	0.819	38276.1461
304.137319	1.99361	4.83	0.514	61083.2830
304.136802	1.99843	4.65	0.214	147069.926
304.136337	1.97729	4.45	0.036	864978.331

ACKNOWLEDGMENTS

The authors acknowledge the assistance given by all who contributed to this work, especially B. Pieperbeck, for performing a part of the measurements, and P. Claus and H.-J. Collmann, for carrying out parts of the computational work. Above all, the authors thank the Deutsche Agentur für Raumfahrtangelegenheiten GmbH (DARA) for financial support of this work under Grant 50 QV 9052.

REFERENCES

1. H.-G. Kratz and W. Wagner, *Meßapparatur zur Druck-, Dichte-, Temperatur-(p, v, T)-Messung im kritischen Gebiet reiner fluider Stoffe*, Forsch.-Ber. BMFT W 85-006 (BMFT, Bonn, 1985).

2. N. Kurzeja, *Entwicklung und Aufbau einer Meßapparatur nach der ppT-Mehrzellenmethode zur Messung des thermischen Zustandsverhaltens im kritischen Gebiet reiner fluider Stoffe*, Dissertation Ruhr-Universität Bochum (Bochum, 1990).
3. W. Wagner, N. Kurzeja, and B. Pieperbeck, *Fluid Phase Equil.* **79**:151 (1992).
4. W. Wagner, N. Kurzeja, and Th. Tielkes, in *Abstracts of the Ninth European Symposium of Gravity-Dependent Phenomena in Physical Sciences* (Berlin, 1995), pp. 81–82.
5. Th. Tielkes, N. Kurzeja, and W. Wagner, *Präzisionsmessungen der thermischen Zustandsgrößen im kritischen Gebiet von Kohlendioxid*, Fortschr.-Ber. VDI, R 3, Nr. 488 (VDI-Verlag, Düsseldorf, 1997).
6. Th. Tielkes, N. Kurzeja, and W. Wagner, To be submitted for publication.
7. Th. Tielkes, N. Kurzeja, and W. Wagner, To be submitted for publication.
8. N. Kurzeja, Th. Tielkes, and W. Wagner, To be submitted for publication.
9. R. Gilgen, R. Kleinrahm, and W. Wagner, *J. Chem. Thermodyn.* **24**:1243 (1992).
10. P. Nowak, Th. Tielkes, R. Kleinrahm, and W. Wagner, *J. Chem. Thermodyn.* **29**:885 (1997).
11. D. S. Canell, *Phys. Rev. A* **12**:225 (1975).
12. J. H. Lunacek and D. S. Canell, *Phys. Rev. Lett.* **27**:841 (1971).
13. G. T. Feke, G. A. Hawkins, J. B. Lastovka, and G. B. Benedek, *Phys. Rev. Lett.* **27**:1780 (1971).
14. D. A. Balzarini, *Can. J. Phys.* **50**:2194 (1972).
15. R. Hocken and M. R. Moldover, *Phys. Rev. Lett.* **37**:29 (1976).
16. K. Morofuji, K. Fuji, M. Uematsu, and K. Watanabe, *Int. J. Thermophys.* **7**:17 (1986).
17. D. Y. Ivanov, in *Proceedings of the Eleventh International AIRAPT Conference, Vol. 2* (Le Creusot, 1979), pp. 713–714.
18. J. M. H. Levelt Sengers, B. Kamgar-Parsi, F. W. Balfour, and J. V. Sengers, *J. Phys. Chem. Ref Data* **12**:P1 (1983).
19. A. Abbaci and J. V. Sengers, *An assessment of the thermodynamic properties of sulfurhexafluoride in the critical region*, Technical Report No. BN 1111 (University of Maryland, 1990).
20. Z. Y. Chen, A. Abbaci, S. Tang, and J. V. Sengers, *Phys. Rev. A* **42**:4470 (1990).
21. L. A. Makarevich, O. N. Sokolova, and A. M. Rozen, *Sov. Phys.-JETP* **40**:305 (1974).
22. J. V. Sengers and J. M. J. van Leeuwen, *Physica A* **116**:345 (1982).
23. J. V. Sengers and J. M. J. van Leeuwen, *Int. J. Thermophys.* **6**:545 (1985).